Multiterminal High-Voltage dc Systems with Series-Parallel Valve Group-Based High-Voltage dc Substations

Sreenivasa S Jaldanki
Oak Ridge National Laboratory
Knoxville, TN, USA
jaldankiss@ornl.gov

Suman Debnath
Oak Ridge National Laboratory
Knoxville, TN, USA
debnaths@ornl.gov

***Abstract*—To transfer large amount of power over long distances, multiterminal direct current (MTdc) system based on bipole high-voltage direct current (HVdc) technology is a viable option. However, such system results in large dc transmission loss. The same can be reduced by increasing the dc voltage level. This paper introduces a new MTdc system architecture comprising of series (for increasing dc voltage level) and parallel (for increasing dc current capability) connected HVdc converters. The new architecture is compared with the bipole MTdc architecture in terms of equipment needed and dc transmission loss. The control modifications needed for the MTdc system are identified and the performance of the developed control is verified through electromagnetic transient (EMT) simulations.**

Keywords*—*high-voltage dc converter, multiterminal dc system, parallel connection, series connection.

I. Introduction

Multiterminal high-voltage dc (MTdc) systems are expected to play a significant role in modernizing the US electrical power grid [1]. Such systems can enable large power transfer between US asynchronous ac grids and will be able to help transfer the power generated by new energy resources over long distances. In [2], a new mixed monopole and bipole MTdc architecture, which enables step-by-step expansion of the MTdc network and enhanced operational flexibility, is introduced. Recent report [3] points out that future energy generators will be able to generate power of the order of a few tens of gigawatts. These works emphasize the necessity of MTdc systems and high-voltage dc (HVdc) substations, which can handle large power. Today, 5 GW is the maximum power rating of the existing voltage source converter (VSC)–based HVdc substation, which connects the modular multiterminal converter (MMC)–based valve groups (VGs) in series and in parallel manner [4]–[8]. A new VSC HVdc substation topology, named bipolar substation (BPS), is presented in [9] for ultra–high voltage dc, which introduces additional overhead lines (OHLs) at the junction of the series-connected VGs such that the single largest contingency is restricted to the power rating of a single VG.

This paper presents an MTdc system with four HVdc terminals employing the concept of a BPS. The MTdc system is capable of transferring 24 GW of power between different terminals. Electromagnetic transient (EMT)–based simulation results are provided to prove the stable operation of the MTdc system during steady state and during the maintenance of VGs. The advantages of the proposed architecture compared with a standard bipole architecture in terms of the amount of equipment needed and transmission loss are analyzed.

The paper is organized as follows. The proposed MTdc system architecture is explained in section II. The control block diagram used for the MTdc system and additional control loops required for stable operation of the system are detailed in section III, followed by the simulation results in section IV. In sections V and VI, the proposed and the standard MTdc architectures are compared in terms of equipment needed and transmission system loss. The conclusions are presented in section VII.

II. MTdc Architecture

As per the studies based on capital expenditure model, four locations in eastern interconnection (EI) power network of the USA which require large power transfer are identified. The details are presented in Fig. 1 and Table I. The power requirement at each location is in between 4 GW to 20 GW, while it is to be transferred over hundreds of miles as shown in Table I.

To address the problem of large power transfer over long distances, a new MTdc system architecture based on the BPS substation [9] is utilized. The schematic diagram of the MTdc system is shown in Fig. 2.

Fig. 1. HVdc terminals in EI network of the USA.

Each substation is formed using series- and parallel-connected VGs [9] rated for 2 GW and 400 kV dc voltage [4]-

[8]. A VG comprises a half-bridge modular multilevel converter. Each arm of the VG comprises 200 series-connected half-bridge submodules each rated for 2 kV. The submodule capacitance is 28 mF, which corresponds to an energy storge of 33.3 kJ/MVA. The VG is connected to the ac grid through a 220/220 kV star (grid side)/delta (VG side) transformer. The leakage inductance of the transformer is 15%, and the arm inductance is 12% of 2 MVA base. On the ac side, all the VGs of a BPS are connected in parallel. Th ac grid is represented by an ideal voltage source.

TABLE I. POWER RATING of HVdc SUBSTATIONS

Location	Power (GW)	Mode			Distance (mi)
Grand Island (GI)	16	Rectifier		GI to FD	312
Fort Dodge (FD)	8	Rectifier		FD to CHI	611
Chicago (CHI)	4	Inverter		CHI to DET	283
Detroit (DET)	20	Inverter			

Five OHLs operating at potentials of +800 kV, +400 kV, neutral, −400 kV, and −800 kV are responsible for power transfer between the HVdc substations. The Grands Island (GI) and Detroit (DET) BPSs are connected with OHLs at all five dc voltage levels. Because the BPSs at Fort Dodge (FD) and Chicago (CHI) have smaller power ratings, they are connected with the ±400 kV and neutral buses only. To meet the power demand, at the DET location, two separate VGs (VG+L3 and VG-L3) are included with an OHL of length 10 mi. The MTdc system is grounded at the GI substation.

For the design of the MTdc system, the power flow scenario shown in Fig. 2 was considered. A total of 24 GW of power flows from the GI and FD substations to the CHI and DET substations. The currents through different sections of OHL under these conditions are shown in Fig. 2. Each OHL section of the MTdc network is assumed to be rated for 5 kA dc current. Hence, based on the required dc current capacity, in between different BPSs, OHL sections of 5 kA rating are connected in parallel. The neutral bus is also rated for 5 kA. The 312 mi, ±400 kV lines between the GI and FD substations do not carry any current during the considered power flow scenario. However, those lines are essential in case of VG maintenance as detailed in section IV.

Though not shown in the figure, to break the dc fault current, two dc breakers (DCBs) of 5 kA continuous current rating must be connected across each end of the OHL section. Hence, 28 DCBs are required. In this work, the dc fault study was not considered, and thus DCBs were not included in the simulation model.

III. CONTROL BLOCK DIAGRAM

The block diagram of the control implemented for each VG is shown in Fig. 3. Reference commands are provided for the ac real power, reactive power, dc voltage, and the sum of the submodule voltages of the VG. The internal stored energy of the VG is controlled by controlling the q component of the ac current, I_{qX}^* [10]. The dc voltage is controlled through the active current component, I_{qY}^*. The reactive power reference is converted into an equivalent current reference, I_d^*. Internal d-q current loops control the ac current to their respective references. The circulating current controller maintains the second harmonic component of arm currents at zero.

To enable series and parallel operation of VGs, two additional loops marked by shaded region in Fig. 3 are added [9]. The controller marked as 'Parallel Connection' avoids 120 Hz current oscillations between the parallel-connected VGs by controlling the nonzero frequency common-mode arm current to zero.

Further, unequal power sharing between the series-connected VGs is observed when the OHL at +400 kV is absent (because of dc fault or maintenance of OHL). To correct the unequal load sharing, an additional controller named 'Series Connection' (see Fig. 3) is included [9]. As shown in Fig. 3, the ac power reference of the series-connected VGs is adjusted based on the difference between the dc voltages of the VGs.

At the MTdc system level, the power balance is maintained through the dc voltage droop control [11]. All the VGs in the MTdc system are provided with active power reference. Based on the error in active power, the dc voltage reference is drooped/adjusted through a proportional controller. The error in active power is not strictly controlled to zero. Hence, the power transferred between different substations might partially deviate from the respective reference power commands. The total power loss of the MTdc system is shared among all the VGs.

IV. SIMULATION STUDY

In this section, the MTdc systems in Fig. 2 is simulated using EMT based simulation software. Simulation studies are performed to verify the energization process and steady state operation of the MTdc system. In the large MTdc system, periodic maintenance of equipment is essential. During maintenance, the MTdc system should be able to operate with minimum loss of power transfer capability. Hence, operation of MTdc system under maintenance of VGs in various substations is also studied.

The system parameters of the VG are shown in Table II. The OHLs were modeled by the ±400 kV dc lines of [12]. Whereas in [12], each OHL tower contained two conductors (one conductor at +400 kV and another at −400 kV), in this work, both the conductors of the tower were connected in parallel at a single potential, such that the ampacity was 5 kA. Hence, three separate towers existed for the +400 kV, neutral, and −400 kV lines. Because no benchmark model was available at 800 kV potential, in this work, the tower and the conductor models used for the 400 kV OHL were replicated for the 800 kV OHL.

A. Power Flow in Fig. 2

The simulation results for the ac power transferred through the four HVdc SSs (which corresponds to the scenario in Fig. 2) are shown in Fig. 4(a). All the VGs of the four SSs supplied reactive power (roughly 33% of 2 GVA) to the ac grid (Fig. 4[b]). Note that DET1 and DET2 in Fig. 2 are together considered a single SS in the results presented in the following figures.

The dc voltages (measured with respect to the ground) at various nodes of the MTdc system are presented in Fig. 5. At $t = 0$ s, the ac breakers of all the VGs were closed. The submodules of the VGs, and the entire dc OHL were charged

through a pre-insertion resistance. At $t = 0.5$ s, the pre-insertion resistance was bypassed. At $t = 0.75$ s, the VGs were deblocked, the dc voltage was ramped up to the nominal value, and the energization process was completed. Note that the dc OHL was charged by all the VGs simultaneously.

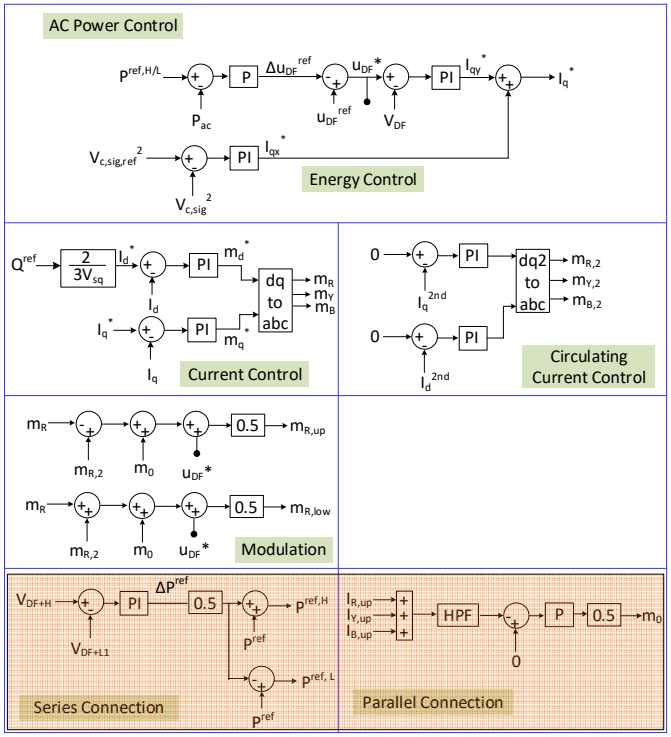

Fig. 3. Control block diagram of the MTdc system.

TABLE II SYSTEM PARAMETERS OF VGS

Grid voltage	220 kV
Transformer	2 GW, star (grid side)/delta (VG side) transformer, 220/220 kV, 15% leakage indutance
VG	2 GW, 400 kV dc 200 half-bridge sub-modules per arm, each rated for 2 kV 12% arm inductance 28 mF capacitor per sub-module

At 1.75 s, the active power reference of all the VGs was ramped up at a rate of 2 GW/s. Because of the droop control, during the ac power ramp-up, the dc voltage of the rectifier increased, and the dc voltage of the inverter substations decreased, as shown in Fig. 5. Once the power ramp-up was completed, the dc voltages reached a steady state.

The dc power transferred through each VG of the MTdc system is presented in Fig. 6. In the GI and FD substations, the power was negative (rectifiers), and in the CHI and DET substations, it was positive (inverters). Based on the droop control and the total system loss, different VGs of a SS operated at different dc powers (the difference was very small).

However, the total MTdc operated under a balanced condition, and the neutral current was zero, as shown in Fig. 7. As an example, the dc current through the OHL section between FD and CHI is shown in Fig. 7. The neutral current in all other OHL sections was also observed to be zero.

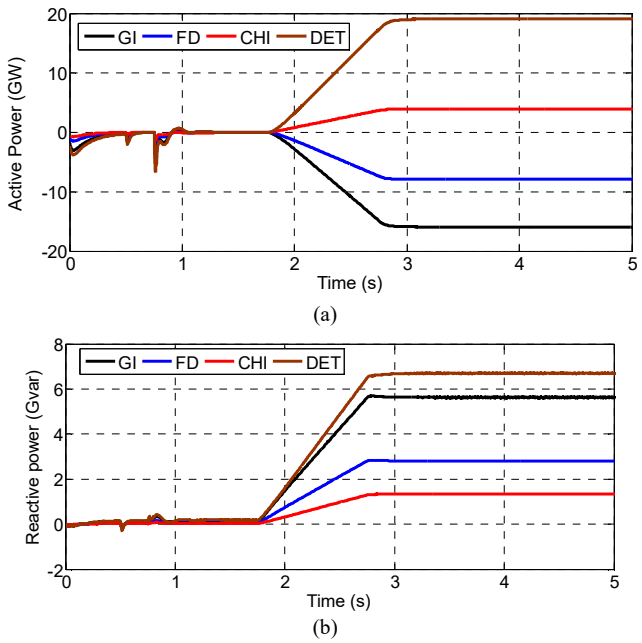

Fig. 4. Power transfer between various SSs of the MTdc network: (a) active power (negative indicates rectifier operation) and (b) reactive power.

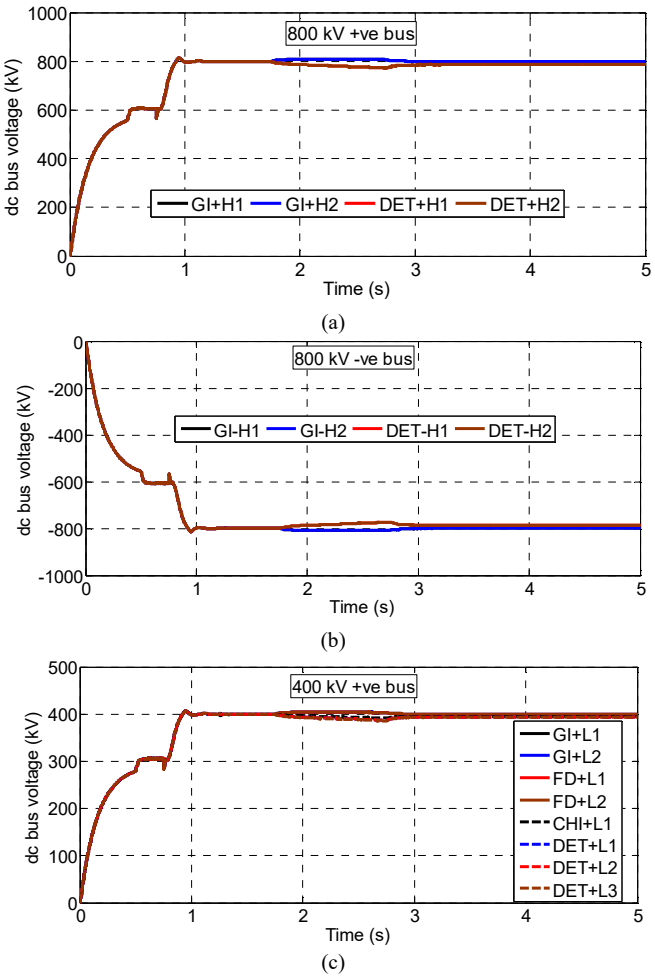

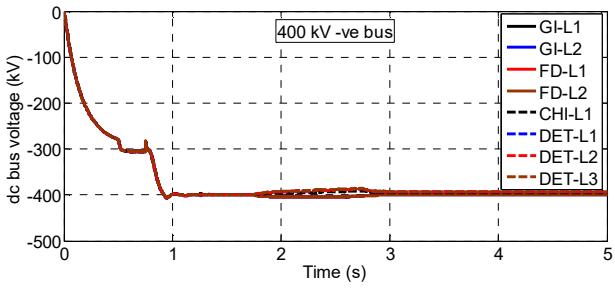

(d)

Fig. 5. dc bus voltages at various VGs: (a) 800 kV +ve bus, (b) 800 kV −ve bus, (c) 400 kV +ve bus, and (d) 400 kV −ve bus.

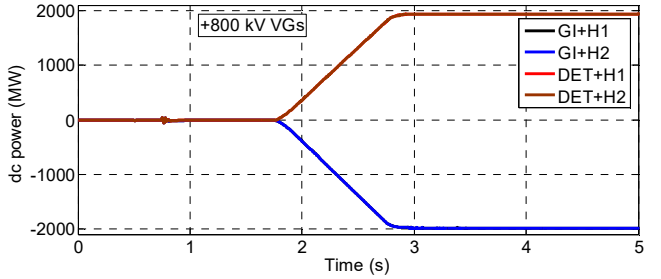

(a)

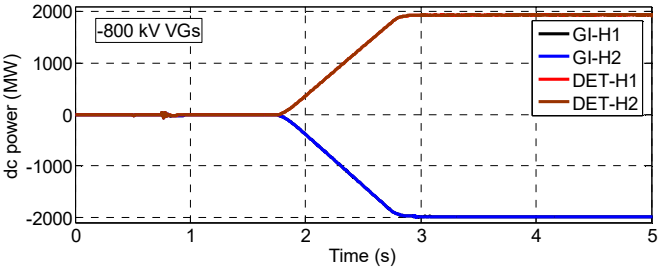

(b)

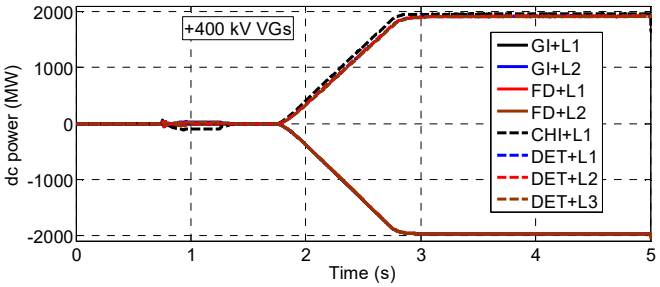

(c)

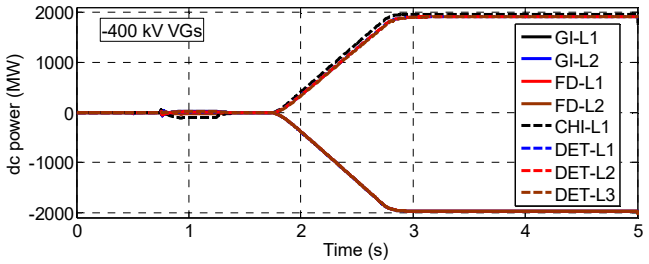

(d)

Fig. 6. dc power transferred through various VGs connected to (a) +800 kV bus, (b) −800 kV bus, (c) +400 kV bus, and (d) −400 kV bus.

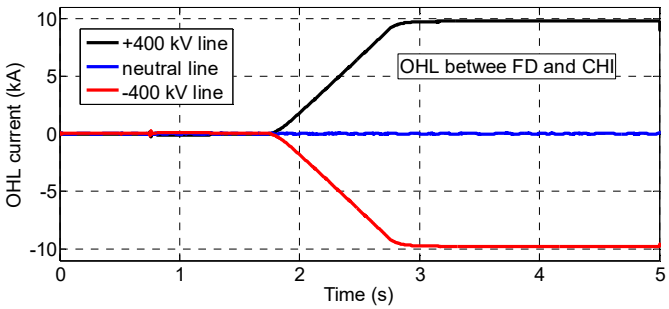

Fig. 7. Current through OHL between FD and CHI.

B. *Maintenance-1*

In this simulation, the VG+L2 of SS FD, which is supposed to act as a rectifier, was assumed to have been under maintenance. Hence, gate pulses for that VG were blocked. To maintain power balance, the ac power command to VG+L2 in DET SS was set to zero. All the other VGs operated under the same conditions as in section IV.A.

Because the power flows in the positive and negative parts of the MTdc system were unbalanced, as shown in Fig. 8(a), the currents through the +400 kV and −400 kV OHLs between FD and CHI differed, resulting in large neutral current. To handle these sort of maintenance scenarios, the neutral OHL was designed to carry 5 kA continuous current. The case proves the necessity of designing the neutral conductor of the system to carry dc current equivalent to the rating of one VG.

Though the VG+L1 in CHI did not transfer any active power, it supported the ac grid by supplying reactive power (STATCOM mode) as shown in Fig. 8(b).

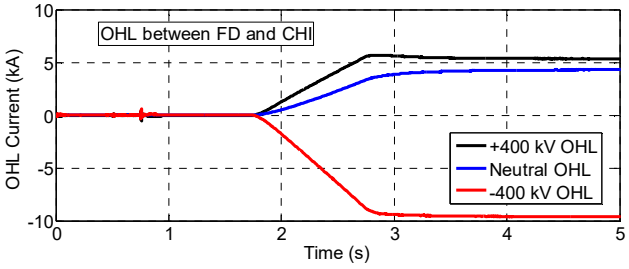

(a)

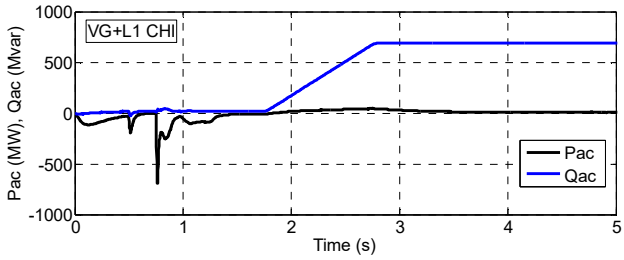

(b)

Fig. 8. Maintenance of VG+L2 in FD: (a) current through the OHLs between FD and CHI and (b) active and reactive powers of VG+L1 in CHI.

C. *Maintenance-2*

This section covers the maintenance event of the VG+L2 of the GI substation. In the simulation study, the gate pulses for this VG were blocked to mimic the maintenance scenario. To

main power balance, the active power reference to the VG+L2 of DET SS was set to zero.

The simulation results for this scenario are presented in Fig. 9. The ideal power flow conditions in this event are presented in Fig. 10. The dc powers handled by the four positive VGs of the GI station are shown in Fig. 9(a). Because VG+L2 was blocked, its dc power was zero. VG+H1 and VG+H2 shared the power equally. The VG+L1 of GI SS handled around 2,100 MW, which is slightly more than its power rating.

Because of the absence of the GI VG+L2, the dc current of the GI VG+H2 returned through the +400 kV OHL as shown in the Fig. 10 and Fig. 9(b). This resulted in a neutral current of around 5 kA throughout the OHL between GI and DET (Fig. 10). However, the neutral current (OHL between GI and FD) from the simulation results reached only up to 4 kA, as is evident from Fig. 9(b). Further, the current through the −400 kV OHL was not equal to zero (Fig. 9[b]).

The parallel-connected VG+L1 and VG+L2 of CHI SS handled different amounts of power. However, because of the employed Parallel Control, such operation did not trigger any 120 Hz oscillations between them, as shown in Fig. 9(c).

The deviation of power and current from ideal power flow presented in Fig. 10 can be attributed in part to the complex structure of the MTdc network and unbalance in power between the positive and negative parts of the network. This behavior can also be attributed to the P_{ac}–V_{dc} droop control, which did not strictly control the power handled by the VGs to their reference value. To conclude, during the absence of a VG, the power transfers through other VGs must be curtailed, or the VGs and other equipment of the MTdc system must be slightly overrated. However, detailed investigations must be performed to understand the effects of all the possible maintenance scenarios on the design of the MTdc network.

V. Standard Bipole Based MTdc System

In the previous sections, the MTdc system with the proposed architecture is discussed. Between various HVdc terminals, the same power transfer capability can be achieved with the help of the commercially available bipole HVdc architecture by connecting various VGs in parallel. In this section, such bipole based MTdc system is designed, and simulation results are presented. Further, to maintain transmission loss equal to that of BPS MTdc system, additional parallel dc overhead lines are added. All these configurations are compared in terms of equipment needed and dc transmission system loss.

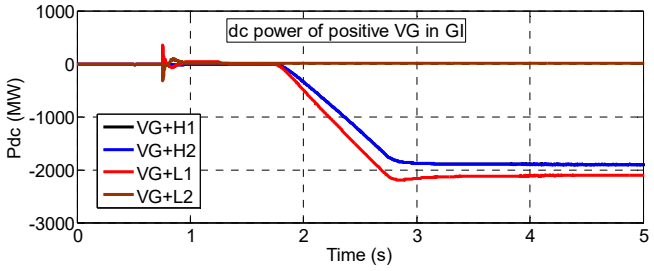

(a)

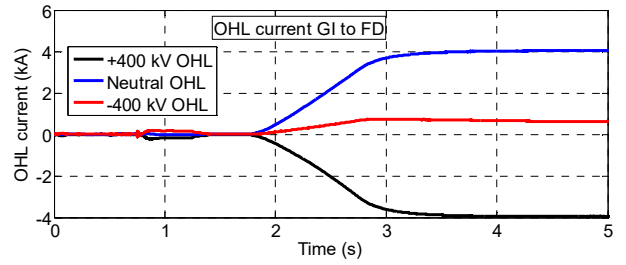

(b)

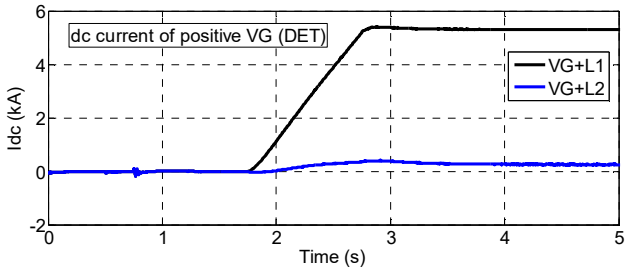

(c)

Fig. 9. Maintenance of the GI VG+L2: (a) dc power of positive VGs in GI, (b) current through the OHLs between GI and FD, and (c) dc current of VG+L1 and VG+L2 in DET.

To achieve 24 GW of power transfer between the four substations of the MTdc system, a standard bipole-based HVdc system must be designed as shown in Fig. 11. Like the system in Fig. 2, each VG is rated for 2 GW. To meet the current demand, four, six, and five parallel OHLs, each rated for 5 kA, are connected between the GI and FD, FD and CHI, and CHI and DET substations, respectively (Case 1). Please note that with this design, maintenance of a VG or an OHL section results in a reduction of only 2 GW power transfer capability. Similar to BPS based MTdc system in section IV, the neutral conductor is to be rated for 5 kA (to handle the asymmetric operation of MTdc system under maintenance of a VG).

The EMT simulation results of the MTdc bipole system are presented in Fig. 12. Along with the standard control algorithm presented in Fig. 3, additional control loop which enables parallel connection of VGs is employed. The power flow conditions between various substations were close to those in Fig. 4(a), though not exactly the same. The difference can be attributed to the dc voltage droop control method (Fig. 3). Because the bipole system operated in a balanced fashion, a neutral current was zero (not presented here).

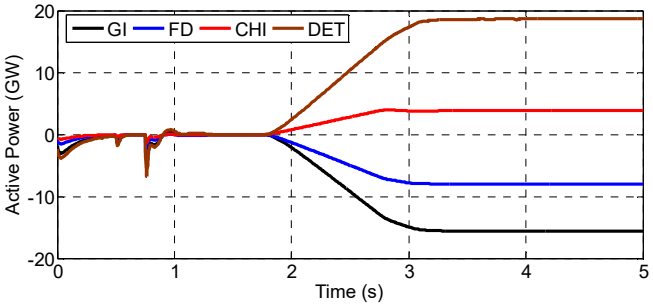

Fig. 12. Power transferred through the MTdc SS in a standard bipole configuration (Case 1).

Table III compares the MTdc systems in Fig. 2 and Fig. 11 in terms of the main equipment needed and insulation

requirements. Though the total numbers of transformers, arm inductors, ac bushings, and dc bushings do not change between the two MTdc systems, the MTdc system in Fig. 2 has greater insulation requirements because few of the pieces of equipment are connected to the 800 kV dc bus. However, with the system in Fig. 2, the number of dc breakers and the length of the OHL needed drastically decrease, resulting in significant savings in capital cost. Further, the copper loss of the dc transmission system is reduced by 38% (neglecting the insulation loss of the OHL).

If the ohmic loss of the transmission system is to be reduced and to be maintained at the same level as that of the system in Fig. 2 (one of the important design criteria used by the system operators for long distance HVdc systems), additional parallel lines are needed, as shown in Fig. 11 (Case 2). As more parallel lines are added, the number of dc breakers and the total length of the OHL drastically increase as indicated in Table III, resulting in large capital cost. The analysis in this section shows that BPS-based MTdc systems are attractive for large power transfer over long distances compared with standard bipole-based MTdc systems. Detailed analysis regarding transmission loss is provided in section VI.

TABLE III. COMPARISON BEWEEN Fig. 2 AND Fig. 11

	Voltage (kV)	Fig. 1	Fig. 11 (Case 1)	Fig. 11 (Case 2)
Transformers	800	8		
	400	16	24	24
Arm inductor	800	48		
	400	96	144	144
ac bushings	800	24		
	400	96	72	72
dc bushings	800	8		
	400	24	24	24
	Neutral	16	24	24
Length of OHL in mi	800	4824		
	400	3654	12658	21116
	Neutral	1206	1206	1206
dc breakers	800	8		
	400	20	60	100
OHL loss		7854 *($I_{dc}^2R_{dc}$)	12658 *($I_{dc}^2R_{dc}$)	7594 *($I_{dc}^2R_{dc}$)

*R_{dc}: the resistance of the OHL per mile

VI. Loss Evaluation

In this section, the losses incurred in the MTdc system with the three MTdc configurations presented in Fig. 2 and Fig. 11 were compared. Table IV presents the power measured through simulation at various MTdc system locations. The MTdc system in Fig. 11, Case 2, was also simulated in the EMT domain, but the simulated waveforms are not presented here.

In Table IV, negative power indicates rectifier operation, and positive power represents inverter operation. At each VG, power was measured at both ac and dc terminals. The difference represents the loss in VG. Note that the majority of the loss in VG occurred in the semiconductor devices, and estimating this loss exactly requires a detailed analysis. Further, the VG loss was very small compared with the power processed by the VG. Nevertheless, the error in VG loss, if any, was uniform throughout all three MTdc configurations and did not affect the comparative loss evaluation of the three MTdc configurations.

Table IV also presents the cumulative measured power of all the VGs within a SS. The sum of the ac powers measured at substations CHI and DET represents the total power delivered by the MTdc system to the ac grid. As already mentioned, the total power delivered to the ac grid differs with different MTdc configurations because of the droop control method adopted. Further, the sum of the dc powers of all four SSs represents the total power loss incurred in the OHL of the MTdc system.

Because the total power delivered to the ac system differed with different configurations, the loss factor, which is a ratio of OHL loss to the total ac power delivered, was a good parameter to use to compare the three MTdc systems. As shown in Table IV, the BPS-based MTdc system resulted in a smaller loss factor or less operating cost compared with the system in Fig. 11, Case 1. The capital cost was also less because the total length of the OHL was less. However, cost will increase because of the higher insulation requirements (Table III).

Though the system in Fig. 11, Case 2, is comparable with the Fig. 2 system in terms of operating cost/loss factor, its capital cost is substantially higher due to longer OHLs and a greater number of dc breakers (Table III). To conclude, the MTdc topology based on BPS is the best choice of the three configurations.

VII. Conclusions

This paper introduces a four-terminal MTdc system based on HVdc BPSs. The MTdc network can transfer 24 GW of power between the HVdc substations over 1,200 mi. The stable operation of the MTdc network during steady state and during maintenance of different VGs was proved through EMT simulations.

Simulations proved that the new MTdc architecture reduces the transmission loss compared with the standard bipole MTdc architecture for the same amount of power transferred. Further, the proposed topology reduces the number of components and the length of dc OHLs, reducing capital cost.

Acknowledgments

The authors would like to acknowledge support from Andre Pereira from the Transformer Resilience and Advanced Components (TRAC) program, Office of Electricity (OE), U.S. Department of Energy (DOE). This material is based upon work supported by DOE's OE TRAC program.

TABLE IV. Power Loss in MTdc system

		Fig. 1	Fig. 2 (Case1)	Fig. 2 (Case2)
P_{ac} (MW)	GI	-15972	-15641	-15859
	FD	-7996	-7997	-8032
	CHI	3870	3812	3863
	DET	19108	18640	19046
Total output power delivered, P_{out} (MW)	P_{ac} of CHI+DET	22978	22452	22909
P_{dc} (MW)	GI	-15833	-15496	-15716

		Fig. 1	Fig. 2 (Case1)	Fig. 2 (Case2)
P_{ac} (MW)	GI	-15972	-15641	-15859
	FD	-7996	-7997	-8032
	CHI	3870	3812	3863
	DET	19108	18640	19046
	FD	-7920	-7928	-7960
	CHI	3906	3848	3896
	DET	19629	18786	19218
OHL Loss P_{OHL} (MW)		578	790	562
% Loss factor	100*(P_{OHL} / P_{out})	2.52	3.52	2.45

REFERENCES

[1] S. Debnath et al., "Models and methods for accessing the value of HVdc and MVdc technologies in modern power grids," GMLC annual report, Sep. 2019, Department of Energy, USA, Pub 124776.

[2] S. S. Jaldanki, S. Debnath, J. Zhang, P. Brown, and J. Novacheck, "Mixed monopole and bipole MTdc architecture," 2023 IEEE Energy Convers. Congr. Expo. (ECCE), Nashville, TN, USA, 2023, pp. 823–829.

[3] J. Ho et al., "Regional energy deployment system (ReDES) model documentation: Version 2020," June 2021, National Renewable Energy Laboratory, USA, NREL/TP- 6A20-78195.

[4] H. Rao, Y. Zhou, S. Xu, and Z. Zhu, "Research and development of ultra-high-voltage VSC for multiterminal hybrid ±800 kV HVdc project in China southern power grid," in CIGRE 2018 Paris Session, 2018, CIGRE.

[5] Y. He, W. Xianf, B. Ni, X. Lu, and J. Wen, "Impact of strength and proximity of receiving AC systems on cascaded LCC-MMC hybrid HVdc system," in IEEE Trans. Pow. Deliv., vol. 37, no. 2, pp. 880–892, April 2022.

[6] F. Cheng *et al.*, "A comprehensive AC fault ride-through strategy for HVDC link with serial-connected LCC-VSC hybrid inverter," in *CSEE J. Power Energy Syst.*, vol. 8, no. 1, pp. 175–187, January 2022, doi: 10.17775/CSEEJPES.2020.03510.

[7] H. Rao *et al.*, "Key technologies of ultra-high voltage hybrid LCC-VSC MTDC systems," in *CSEE J. Power Energy Syst.*, vol. 5, no. 3, pp. 365–373, September 2019, doi: 10.17775/CSEEJPES.2019.01140.

[8] H. Ying, H. Weihuang, L. Ming, and L. Tao, "Steady-state control strategy of multi-terminal hybrid UHVDC," *2017 19th Eur. Conf. Power Electron. Appl. (EPE'17 ECCE Europe)*, Warsaw, Poland, 2017, pp. P.1–P.10, doi: 10.23919/EPE17ECCEEurope.2017.8098954.

[9] S. S. Jaldanki and S. Debnath, "A new HVdc substation architecture with higher power transfer capability," 2024 IEEE Power Energy Soc. Gen. Meet. (PESGM), to be held at Seattle, Washington, USA, 21–25 July 2024.

[10] S. Wang, G. P. Adam, A. M. Massoud, D. Holliday, and B. W. Williams, "Analysis and assessment of modular multilevel converter internal control schemes," in *IEEE J. Emerg. Sel. Top. Power Electron.*, vol. 8, no. 1, pp. 697–719, March 2020, doi: 10.1109/JESTPE.2019.2899794.

[11] J. Beerten, S. Cole, and R. Belmans, "Modeling of multi-terminal VSC HVDC systems with distributed DC voltage control," in *IEEE Trans. Power Syst.*, vol. 29, no. 1, pp. 34–42, January 2014, doi: 10.1109/TPWRS.2013.2279268.

[12] CIGRE working group B4.57, Guide for the Development of Models for HVdc Converters in a HVdc Grid, CIGRE, December 2014.

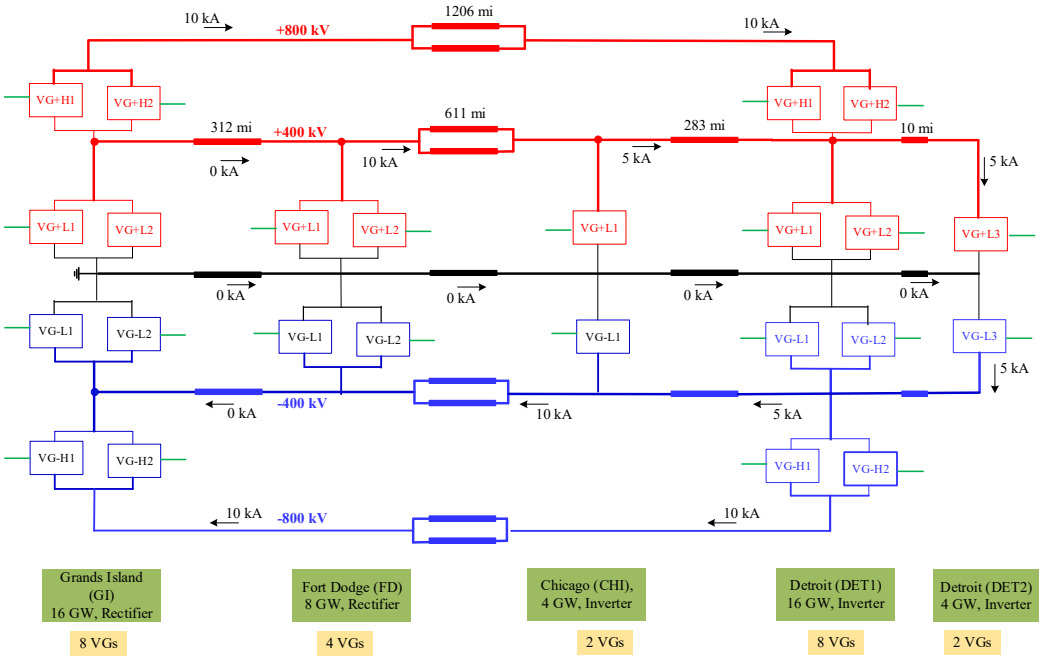

Fig. 2. Four-terminal MTdc system based on BPS substations.

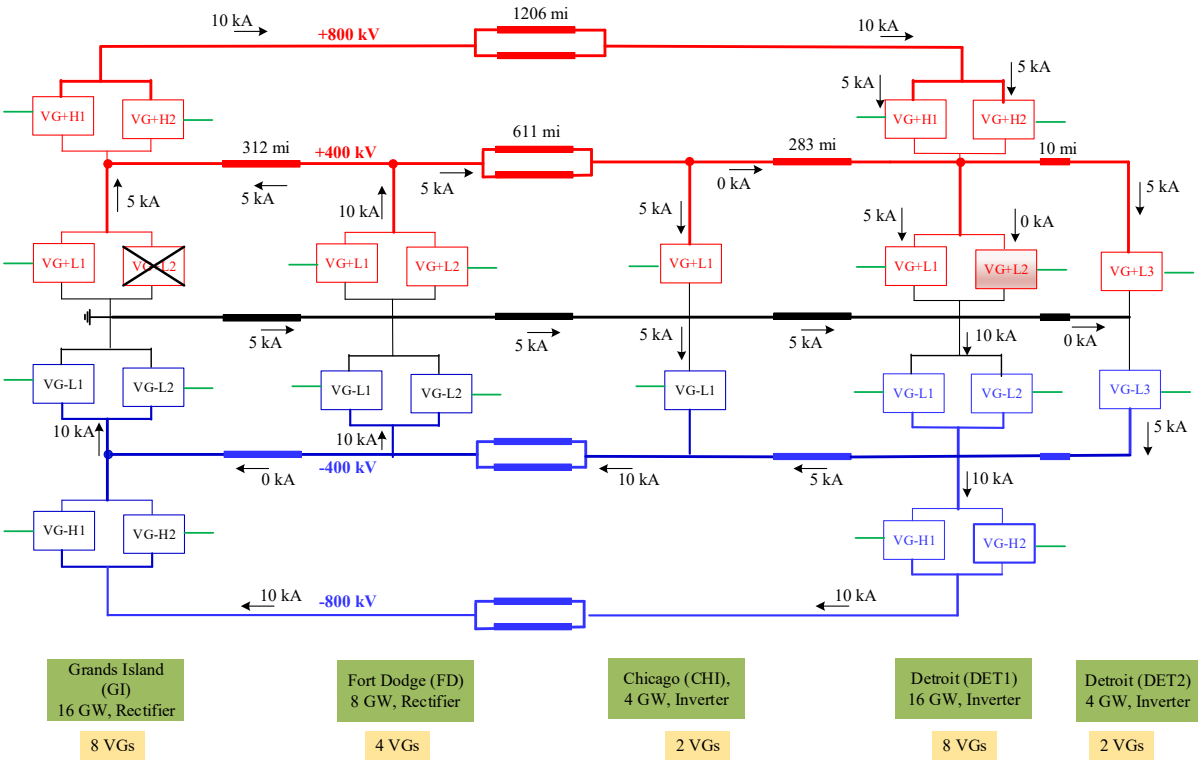

Fig. 10. Power flow scenario under the maintenance of VG+L2 in GI.

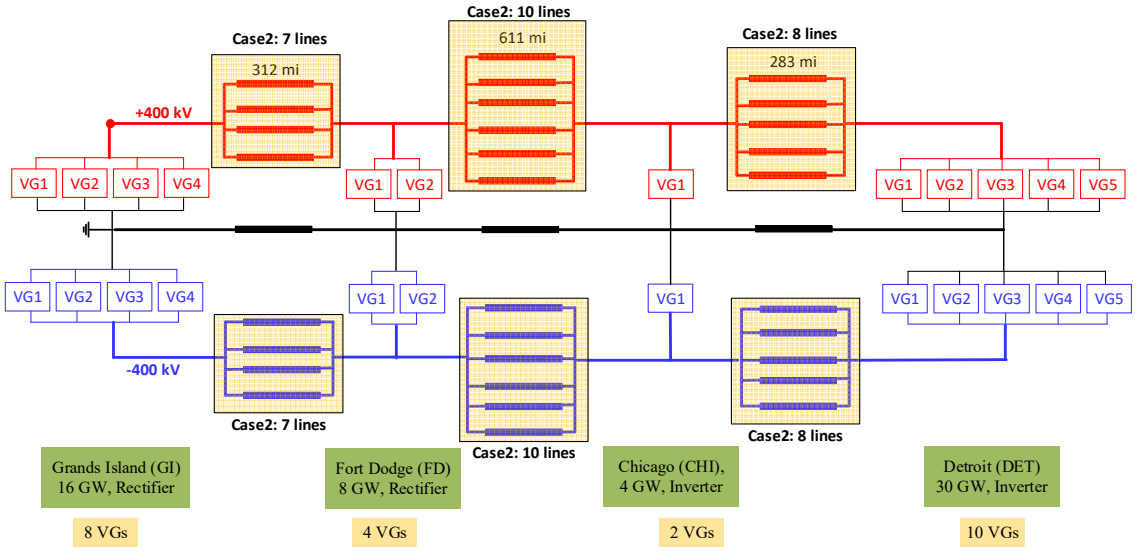

Fig. 11. MTdc system based on a standard bipole configuration.